

Regular Article

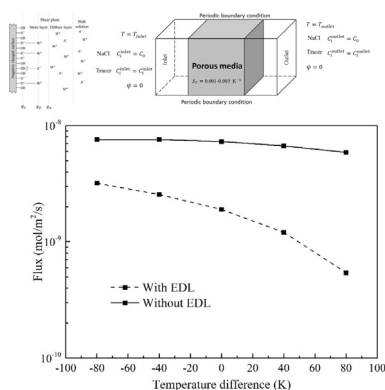
Pore-scale study of thermal effects on ion diffusion in clay with inhomogeneous surface charge

Yuankai Yang, Moran Wang*

Department of Engineering Mechanics and CNMM, Tsinghua University, Beijing 100084, China



GRAPHICAL ABSTRACT



ARTICLE INFO

Article history:

Received 29 September 2017

Revised 25 November 2017

Accepted 17 December 2017

Available online 18 December 2017

Keywords:

Soret coefficient

Thermal effect

Electrokinetic transport

Inhomogeneous charged surface

Compacted clay

ABSTRACT

A better understanding of thermal effect on ion transport in compacted clay is of great significance to enhance long-term safety of repository for high-level radioactive waste. It was reported that the macroscopic Soret coefficient in clay is five times larger than that in free water, which was ascribed to the electrokinetic effect. By pore-scale simulations using lattice Boltzmann method, it is found that the Soret effect contributes little to the ionic flux changes in clay because the Soret coefficient is still around the value in free water for different external temperature gradients. The essential cause is the inhomogeneous charged liquid-solid interfaces in clays induced by the temperature gradient. This interface effect plays an important role to the significant changes of inner electrical and concentration fields in clay. Therefore the concentration diffusion and electromigration should be responsible for this phenomenon instead of the thermodiffusion (Soret effect). This study may improve the understanding of ion transport in clays driven by multiphysiochemical effects.

© 2017 Elsevier Inc. All rights reserved.

1. Introduction

The compacted clay of low permeability is commonly used as the barrier material for the geological disposal of high-level

radioactive waste [1,2]. A better understanding of properties of these materials is of great significance to system design and enhancement of long-term safety of repository [3–6]. In general, the half-life of high-level radioactive waste is very long and the decay of radionuclides continually releases energy. Therefore the high-level radioactive waste likes a heater and continuously heats surrounding buffer materials, which creates a distinct thermal gradient in near field [7,8]. This thermal gradient can affect the

* Corresponding author.

E-mail address: mrwang@tsinghua.edu.cn (M. Wang).

chemical environment and the transport process of radionuclides in compacted clay significantly [9–11], so that the thermal and chemical coupled transport processes have been investigated at different scales. For instance, Thomas et al. provided a theoretical framework to investigate the ion reactive transport in clays under coupled thermal and chemical conditions at macroscale and they found that the temperature gradient could significantly influence the ion transport behavior and concentration distribution in clays [12]. Xie et al. also simulated the chemical diffusion under thermal conditions on continuous scale. Their results showed that the heat transfer and temperature-dependency of diffusion coefficient could enhance the chemical transport process [13].

In the absence of a concentration gradient, when one applies an external temperature gradient in NaCl electrolyte, the thermal motion for a given ion in the high temperature side increases, and therefore the ion gets more collisions from the high-temperature side than from the low temperature side. As a result, the species diffuse from high to low temperature. This effect is called as thermodiffusion (the Soret effect) [14]. For the diluted concentration, in general, a linear relationship between the ionic flux \mathbf{J}_T and the temperature gradient ∇T is assumed as: $\mathbf{J}_T = -D_T \nabla T$, where D_T denotes the thermodiffusion coefficient ($\text{m}^2 \text{s}^{-1} \text{K}^{-1}$) [15]. The Soret coefficient, S_T (K^{-1}), which is usually used to characterize the magnitude of thermodiffusion, is defined as the ratio $S_T = D_T/D$, where D denotes the ionic pure diffusion coefficient. The Soret coefficient could be positive or negative depending on the sense of migration of the reference component and for usual aqueous electrolyte its absolute value is about $|S_T| \sim 10^{-3} - 10^{-2} \text{K}^{-1}$ [16]. The Soret coefficient is a vital input parameter for the macroscale models to predict radionuclide transport in engineered barrier system. Therefore, for these macroscale models, to give a reasonable and reliable value of Soret coefficient is important in order to design the geological repository and predict its durability.

It was found that, compared with the imposing concentration gradient only, the flux of sodium chloride in compacted clay increased by applying an external temperature gradient superimposed on concentration gradient [17–19]. Researchers contributed this raise to the Soret effect and suggested a large value of the macroscale Soret coefficient for clays, which is five times larger than in the free water. They explained that the electrokinetic effect (or electrical double layer (EDL) effect) coupled with temperature effect in clay on pore scale might enhances the Soret effect and was responsible for the observed large S_T . Up to now, no further explanation and quantitatively analysis have been reported.

To experimentally study the enhanced flux within a temperature gradient in clays at macroscale is expensive and tough, especially when the pore size is very small. The measurements may be resulted from multi-factorial coupling and hard to reveal the mechanism. Numerical modeling therefore provides an efficient way to help people know what is happening at pore scale and clarifies effects from different factors. Therefore, in this investigation, the potential for the enhanced ionic flux within a temperature gradient through compacted clay is examined by using a pore-scale modeling. The diffusion in this study means the ionic flux caused by the concentration gradient and the electromigration means that by electrical field. We want to clarify the Soret effect on the change of flux in clay under a temperature gradient. The inhomogeneous charged surface in clay induced by temperature gradient will be carefully considered in this study, which could significantly change the ionic electromigration and diffusion process in clays.

2. Theoretical models

With the electrokinetic effect considered, when the concentration gradient and temperature gradient fields are applied

simultaneously, the evolution of ion transport on pore-scale in porous media should be governed by following equations:

$$\mathbf{J}_i = -D_i \nabla C_i - D_i \frac{z_i e C_i}{kT} \nabla \psi - D_i S_T C_i \nabla T, \quad (1)$$

$$\frac{\partial C_i}{\partial t} + \nabla \cdot \mathbf{J}_i = 0, \quad (2)$$

where \mathbf{J}_i denotes the mass flux of the i th ion species, D_i the diffusion coefficient of the i th ion species, C_i the concentration of the i th ion species, z_i the i th ion algebraic valence, e the absolute charge of electron, k the Boltzmann constant, ψ the electrical potential, t time and T the absolute temperature. The ions in pore solution near surfaces form the electrical double layer, and the electrical potential on the shear plane is called zeta potential, as shown in Fig. 1. Because the ionic mobility in the Stern layer is near zero, only the ion transport in the diffuse layer is considered in this study. The distribution of the electrical potential ψ is governed by the Poisson equation:

$$\nabla^2 \psi = -\frac{\rho_e}{\varepsilon_r \varepsilon_0} = -\sum_i \frac{N_A e z_i C_i}{\varepsilon_r \varepsilon_0}, \quad (3)$$

where ρ_e is the net charge density, N_A the Avogadro's number, and $\varepsilon_r \varepsilon_0$ the dielectric constant of the pore solution. The temperature evolution is based on the Fourier's law as:

$$\rho c_p \frac{\partial T}{\partial t} = \nabla \cdot (\lambda \nabla T), \quad (4)$$

where ρ , c_p and λ are density, thermal capacity and conductivity of media, respectively.

Eqs. (1)–(4) govern the ion transport process on pore-scale in the situation where the temperature, electrical potential and concentration gradients are presented together in clays.

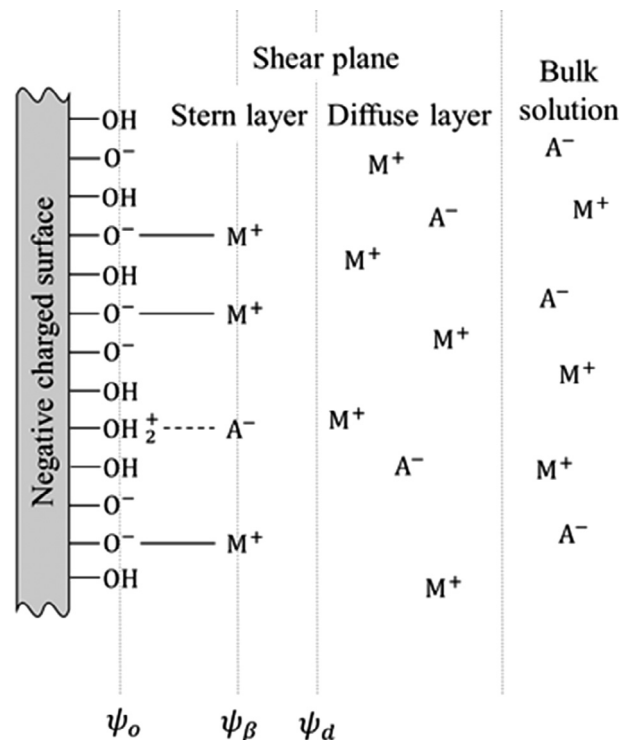


Fig. 1. Sketch of the charged clay particle and electrical double layer. M and A donate the monovalent cation and anion, respectively. ψ_d is the zeta potential. The electrical double layer has two layers: Stern layer and diffuse layer. The Stern layer is also named as compacted layer, which means the counter-ions are compactly adsorbed on the charged surface. In diffuse layer, since the negative charged surface the concentration of cation is higher than the anion.

Since the zeta potential changes with respect to pH, salinity and temperature [10], it is arduous to choose a suitable boundary condition for the electric potential at the liquid-solid interface in clays. Therefore we consider the pH and salinity is constant in clay and apply that the zeta potential is a function only with temperature as the electrical boundary condition: $\psi_d = \zeta(T)$, which is suggested as a linear relationship with temperature by previous theories [20,21]. For the ion transport, the zero normal flux boundary condition is used at the solution-solid interface as: $J_i \cdot \mathbf{n} = 0$.

There are only two temperature dependent terms related to the ionic flux in the governing equations, Eq. (1): one is the term for Soret effect and the other is the electromigration term. In the absence of external electrical field, the magnitude of electrical potential term along ionic transport direction is usually around zero by a previous study [19], hence it seems that the flux raised by adding an external temperature gradient comes from the Soret term. However, if the governing equations (1)–(4) are carefully revisited, there are some temperature-dependent parameters, which may also play a non-negligible role on the change of ion flux in clays. Moreover, the pure diffusion coefficient, dielectric constant, as well as wall electrical potential are all functions of temperature [22], which makes the problem more complicated, and it is hard to conclude without careful evidence that the major change of ion flux is from the Soret term. In the following paragraphs, we will discuss these parameters and analyze the temperature sensitivity of each parameter.

The drift velocity of a given ion in free water is characterized by the diffusion coefficient, which is a very important input parameter for the ion transport model. An approximate dependence of the diffusion coefficient on temperature in liquids is generally predicted by the Stokes-Einstein equation [23]:

$$\frac{D_i(T_1)}{D_i(T_2)} = \frac{T_1 \mu(T_2)}{T_2 \mu(T_1)}, \quad (5)$$

where $\mu(T_1)$ and $\mu(T_2)$ are the dynamic viscosity of the solvent for corresponding absolute temperature T_1 and T_2 . Because the viscosity of water decreases with increasing temperature [24], the diffusion coefficient consequently increases.

The zeta potential is usually used to characterize the electrokinetic effect at the solid-liquid interface. Its value also depends on temperature. For instance, Revil et al. [21] and Wang and Kang [20] suggested a linear relationship for the temperature dependence of the zeta potential on silica by their theoretical models. In addition, Rodriguez and Araujo [10] also carefully measured the zeta potential of quartz, kaolinite and calcite in different temperatures. They found that the zeta potential of kaolinite, a kind of clay, is about -20 mV at room temperature and its value decreases with temperature at a rate -1 mV/°C. It means the absolute value of zeta potential of kaolinite would be double when temperature increases 20 °C from room temperature. Therefore the temperature effect on zeta potential is also significant.

The clay is charged naturally in electrolyte solutions, so the Coulomb force between charged clay surface and ions in pore solution should be considered. Dielectric constant is a basic material property to determine the Coulomb force. The previous studies show that the Dielectric constant of water decreases with increase of temperature [25,26]. The relationship for the temperature dependence of Dielectric constant is given by Malmberg and Maryott [26] as:

$$\varepsilon_r = 87.74 - 0.40008T_c + 9.398 \times 10^{-4}T_c^2 - 1.410 \times 10^{-6}T_c^3 \quad (6)$$

where T_c is the temperature in degrees Celsius.

Table 1 displays the temperature effects quantitatively on each important physical parameter in this study. The concept “temperature sensitivity” for each parameter is defined mathematically as

Table 1
Temperature sensitivity of important physical parameters in this study.

Parameter	Temperature sensitivity, α	Reference
Zeta potential	5%	[10]
Diffusion coefficient	5%	[23,24]
Dielectric constant	0.5%	[26]

its absolute relative rate of variation with respect to temperature change [22]:

$$\alpha = \left| \frac{1}{v} \frac{\partial v}{\partial T} \right|, \quad (7)$$

where v denotes physical parameter. The temperature sensitivity for zeta potential and diffusion coefficient is around 5% but for dielectric constant is only 0.5%. Since the temperature sensitivities for zeta potential and diffusivity are 10 times larger than that for dielectric constant, we only consider the zeta potential and diffusivity with respect to the temperature and ignore the change of dielectric constant by using the average value.

The heat transfer in saturated clays is much faster to reach equilibrium than that for ion diffusion [13]. Because the thermal diffusion coefficient of saturated clays is about 1×10^{-6} m²/s, which is much larger than the ionic diffusivity. Hence the heat transfer is assumed to be steady-state in this study. The previous study indicated that Soret coefficient is not a constant and changes versus salt concentration, temperature and molecule size [15] but this change is not very large. In order to be compared with experiment easily, we still adopt the constant Soret coefficient. Therefore, in this study, two main assumptions have been adopted for the pore-scale modeling, including (i) steady-state heat transfer; (ii) a constant Soret coefficient.

3. Numerical method

This section presents our numerical framework to investigate the Soret effect in clays at pore scale. Benefiting the high efficiency of lattice Boltzmann method (LBM) for parallel computing, there are several successful attempts to use LBM to calculate the ion and temperature evolutions in porous media [27–29]. Therefore, in this investigation, the set of coupled ion and temperature evolution equations in charged clay are solved by the GPU-LBM codes on Tesla K80 GPU [27,30–33].

The corresponding numerical lattice evolution equations for concentration C_i , temperature T and electrical potential ψ are shown as [30]:

$$f_\alpha(\mathbf{r} + c_{f_i} \delta t_f \mathbf{e}_\alpha, t + \delta t_f) - f_\alpha(\mathbf{r}, t) = -\frac{1}{\tau_{f_i}} [f_\alpha(\mathbf{r}, t) - f_\alpha^{eq}(\mathbf{r}, t)], \quad (8)$$

$$g_\alpha(\mathbf{r} + c_g \delta t_g \mathbf{e}_\alpha, t + \delta t_g) - g_\alpha(\mathbf{r}, t) = -\frac{1}{\tau_g} [g_\alpha(\mathbf{r}, t) - g_\alpha^{eq}(\mathbf{r}, t)], \quad (9)$$

$$h_\alpha(\mathbf{r} + c_h \delta t_h \mathbf{e}_\alpha, t + \delta t_h) - h_\alpha(\mathbf{r}, t) = -\frac{1}{\tau_h} [h_\alpha(\mathbf{r}, t) - h_\alpha^{eq}(\mathbf{r}, t)], \quad (10)$$

where f_α , g_α and h_α denote the distribution functions for concentration of i th ion, temperature and electrical potential, respectively. $\tau_{f_i} = 4D_i \delta t_f / \delta x^2 + 0.5$, $\tau_g = 4\lambda \delta t_g / \rho c_p \delta x^2 + 0.5$ and $\tau_h = 4\delta t_h / 4\delta t_h + 0.5$ are corresponding dimensionless relaxation times. \mathbf{r} denotes the position vector, δt corresponding time step, δx lattice size and \mathbf{e}_α the discrete velocities where $\alpha = 0, 1, \dots, 6$ representing the discretized directions for a 3D seventh speed (D3Q7) scheme shown in Fig. 2. For the D3Q7 lattice scheme, the discrete velocities are:

$$\mathbf{e}_\alpha = \begin{cases} (0, 0, 0) & \alpha = 0 \\ (\pm 1, 0, 0), (0, \pm 1, 0), (0, 0, \pm 1) & \alpha = 1 - 6 \end{cases} \quad (11)$$

The equilibrium distribution functions for corresponding evolution equations are [28]:

$$f_{i,\alpha}^{eq} = \omega_\alpha C_i \left[1 - 4D_i \frac{\mathbf{e}_\alpha (e_z \nabla \psi / kT + S_T \nabla T)}{C_i} \right], \quad (12)$$

$$\mathbf{g}_\alpha^{eq} = \omega_\alpha T, \quad (13)$$

$$h_\alpha^{eq} = \omega_\alpha \psi, \quad (14)$$

where the distribution coefficients $\omega_\alpha = 1/4$ for $\alpha = 0$ and $\omega_\alpha = 1/8$ for $\alpha = 1-6$ in D3Q7 system. The concentration, electrical potential and temperature are then calculated respectively as $C_i = \sum f_{i,\alpha}$, $\psi = \sum g_\alpha$, and $T = \sum h_\alpha$. The gradients of potential and temperature can be determined by [28]:

$$\frac{\partial \psi}{\partial x_j} = -\frac{4}{\tau_h \delta x} \sum_\alpha (\mathbf{e}_\alpha \cdot \mathbf{e}_j) h_\alpha, \quad (15)$$

$$\frac{\partial T}{\partial x_j} = -\frac{4}{\tau_g \delta x} \sum_\alpha (\mathbf{e}_\alpha \cdot \mathbf{e}_j) g_\alpha. \quad (16)$$

From Eq. (1), the ionic flux relates to three gradients, thus it is difficult for traditional numerical methods to calculate the local ionic flux in porous media. However, in LBM, the ionic flux is easily obtained by the local distribution functions:

$$\begin{aligned} J_i &= \frac{\tau_{f_i} - 0.5}{\tau_{f_i}} \sum_\alpha C_{f_i, \alpha} f_{i,\alpha} + D_i C_i \left(1 - \frac{\tau_{f_i} - 0.5}{\tau_{f_i}} \right) \\ &\quad \times \left(\frac{e_z}{kT} \frac{\tau_g - 0.5}{\tau_g} \sum_\alpha C_{g,\alpha} g_\alpha + S_T \frac{\tau_h - 0.5}{\tau_h} \sum_\alpha C_{h,\alpha} g_\alpha \right) \end{aligned} \quad (17)$$

The apposite numerical boundary condition is a critical part for the accuracy of simulation. Since the conventional bounce-back rule is easy to handle for complex geometries, it is also used as the zero normal flux boundary condition for ion transport in this study [34]. For the electrical potential boundary, the Dirichlet boundary condition follows [34]: $g_\alpha(\mathbf{r}, t + \delta t_g) - g_\beta(\mathbf{r}, t) = 0.25 \xi(T)$, where the index α and β is the opposite directions normal to the interface and β is the direction towards wall.

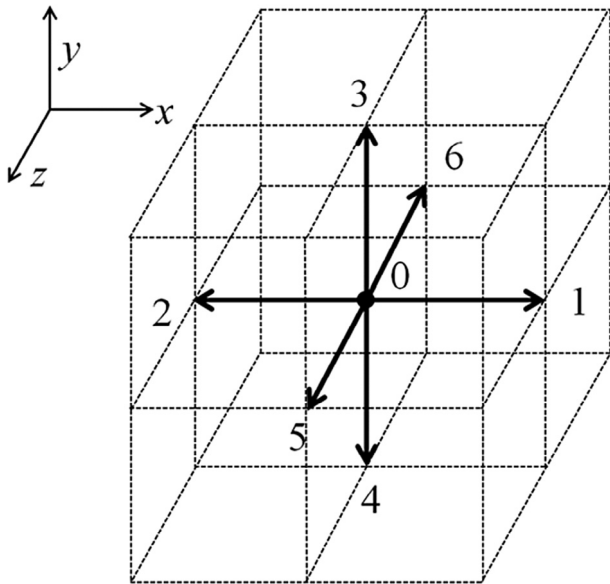


Fig. 2. The discretized directions in D3Q7 model.

The temperature distribution is first obtained by solving evolution equation of LBM, then the coupled Poisson and Nernst-Planck equations are directly solved iteratively in the LBM scheme until the convergences of electrical potential and ion concentrations are reached at each time step of the evolution of ions.

In order to investigate the Soret effect in porous clays by pore-scale modeling, the morphology of the pore structure of clays should be obtained firstly. There are two avenues to get the microstructures of clays: one is the direct measurement of clay microstructures by imaging techniques (such as nano-CT technique) [2,35,36] and the other is numerical regeneration techniques [37,38]. The direct measurement of three dimensional clay microstructures on nanoscale is high-cost and time-consuming [39]. The regeneration strategy is adopted to obtain the three dimensional clay microstructures in this work for fundamental study since its convenience and low cost. To reconstruct the porous microstructures of clays, we employ the QSG algorithm for saturated porous media developed by Wang et al. [27] and the input of this method is the main available structural information such as particle size and porosity.

4. Result and discussion

4.1. Comparison with analytic results

Our numerical framework for ion transport in charged porous media has already been validated in our previous work [39], which indicates the accuracy and robustness of our codes are suitable to capture interactions between ions and charged surfaces. Here to validate our numerical framework for thermodiffusion, we consider a simply one-dimensional (1D) domain to compare the concentration profiles calculated by our numerical method with the analytical model presented by Xie et al. [13], shown in Fig. 3. The length of domain is 0.512 m and the constant diffusivity is employed as $D = 1 \times 10^{-10}$ m²/s. The inlet ion concentration is set as 0.02 mol/L, and the outlet and initial ion concentration is 0.01 mol/L. The other physical parameters are: the Soret coefficient $S_T = 0.2$ K⁻¹, inlet temperature 90 °C and outlet temperature 10 °C. Since the thermal diffusivity is around 10⁻⁶ m²/s, which is four orders of magnitude larger than the ion diffusion, the heat transfer is assumed as steady state. Therefore the temperature gradient is constant that we set $dT/dx = A$, and the analytic solution is:

$$\begin{aligned} \frac{C(x, t) - C_0}{C_1 - C_0} &= \frac{1}{2} \operatorname{erfc} \left(\frac{ADS_T t + x}{2\sqrt{Dt}} \right) \\ &\quad + \frac{1}{2} \exp(-AS_T x) \operatorname{erfc} \left(\frac{-ADS_T t + x}{2\sqrt{Dt}} \right), \end{aligned} \quad (18)$$

where C_1 and C_0 denotes the inlet and initial concentration, respectively. Fig. 3 shows unsteady ion diffusion process in the situation where thermal and ion concentration gradients exist. The good agreements between present simulation and analytic results validate our numerical framework for thermodiffusion.

4.2. Soret coefficient in clay

In this section, we calculate the Soret coefficient in the microstructure of clay by the present numerical framework. Our pore-scale modeling can resolve the pore structure of clays and therefore quantitatively analyses the contribution of each term in Eq. (1) to the flux change as the temperature gradient exists. The microstructure of clay for simulation is a 38.4 nm × 38.4 nm × 38.4 nm cube with two transition regions shown in Fig. 5. This domain size is large enough to satisfy the respective-elementary-volume (REV) requirement for the typical compacted clays. In

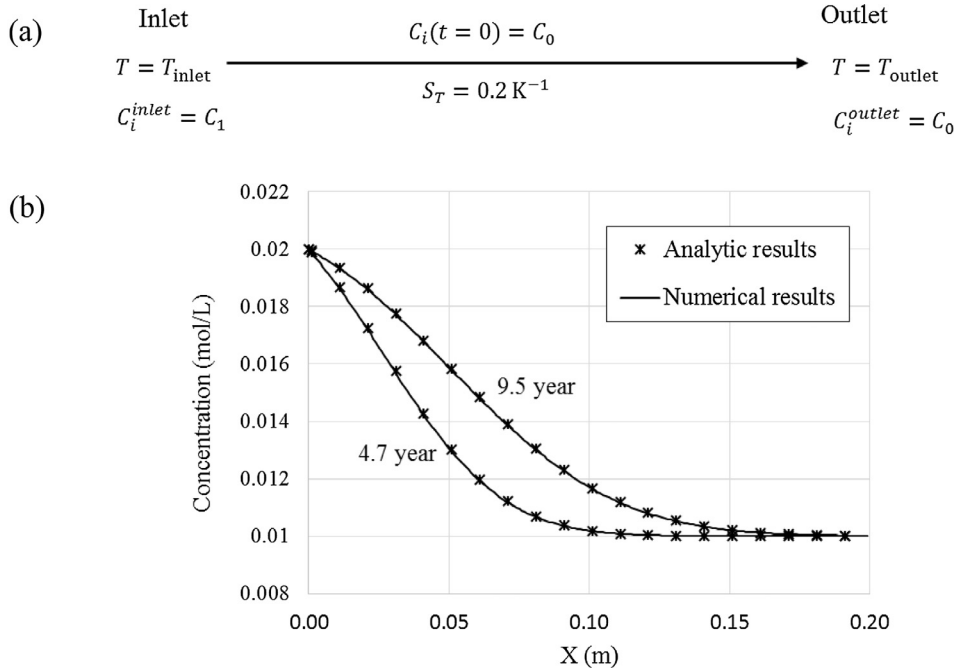


Fig. 3. (a) The computational 1D domain and corresponding initial boundary conditions for validation; (b) comparison of concentration profiles of the simulation with analytic results. The points are analytic results and solid lines numerical results.

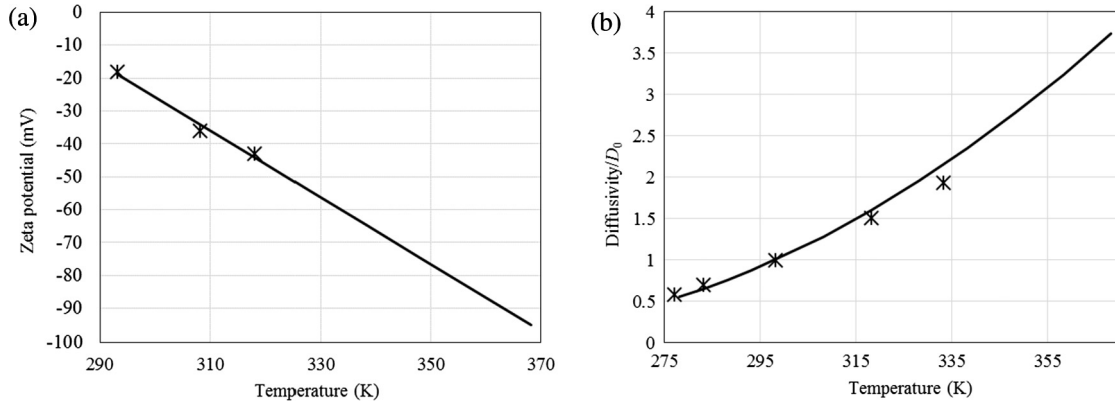


Fig. 4. The zeta potential (a) and diffusivity (b) with respect to temperature. The points in (a) are zeta potentials of kaolinite measured by experiment [10] and the solid line in (a) is the result best fitted with experiment data. The solid line in (b) is the diffusivity normalized by the diffusivity at room temperature calculated by Eq. (5) and the viscosity of free water is used from Ref. [26]. The points in (b) are diffusivities from Ref. [40] to verify the temperature dependency of diffusivity independently.

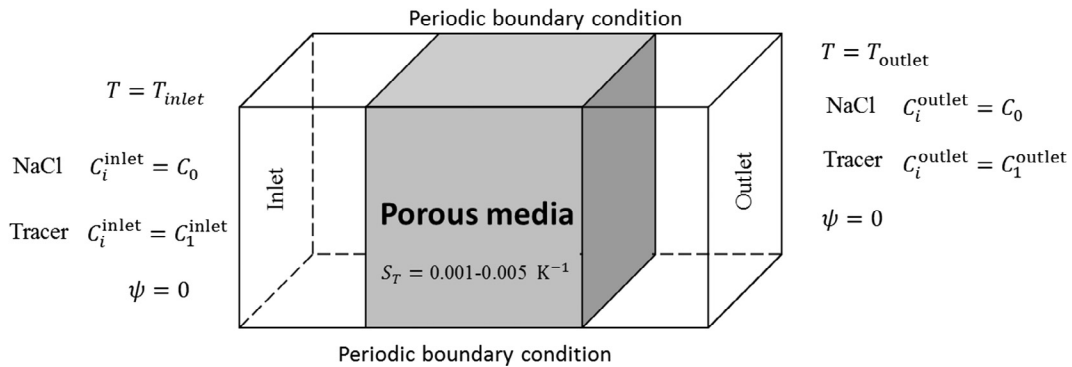


Fig. 5. The sketch of the simulation domain: the microstructure of clay is a 38 nm * 38 nm * 38 nm clay and two transition regions. The corresponding boundary conditions are shown in each sides and the Soret coefficient ranges from 0.001 K⁻¹ to 0.005 K⁻¹.

order to resolve the electrical double layer structure, a $256 \times 128 \times 128$ uniform grid is adopted in our simulation, which is fine enough but does not need too much computational cost. The clay is fully saturated and we consider the solid is not diffusive. To simplify the simulation, we consider the same thermal diffusivities of both solid and pore solution, and the original pore solution in clay is a simple binary monovalent electrolyte solution (e.g. NaCl), which concentration is 0.01 M. The pH and salinity is the same throughout the simulated domain, the changed parameter is the temperature. Hence it is reasonable to assume that the zeta potential of the clay is only related to the temperature. The diffusivities for all ions equal to $1 \times 10^{-10} \text{ m}^2/\text{s}$ at the room temperature 25°C . As mentioned in Section 2, the temperature dependent physical parameters considered in this investigation are the zeta potentials and ionic diffusivities. The detail variations with respect to temperature are presented in Fig. 4. The other parameters are: the dielectric constant $6.95 \times 10^{-10} \text{ C}^2/\text{J} \cdot \text{m}$, and the Soret coefficient $0.001\text{--}0.005 \text{ K}^{-1}$. Because of the cationic chemical adsorption and reaction, the cation diffusion in clays is very complex. This kind of adsorption or reaction is also temperature-dependency, and would affect the transport process and increase the uncertainty. Therefore, in this study, we ignore chemical reaction and use the anion as the tracer to study the thermal effect on ion transport. To refuse the influence of the tracer chloride ion on the salinity and pH of original pore-solution, the concentration of tracer chloride ion is very low as $2 \times 10^{-8} \text{ M}$ at inlet and $1 \times 10^{-8} \text{ M}$ at outlet.

In this simulation, different temperature gradients are applied on clay while the concentration gradient of the tracer is constant and the electrical potential distributions at pore scale are shown in Fig. 6. The electrical potential distributions in different pores are more inhomogeneous in Fig. 6(a) and (c) due to the influence of thermal gradient. Fig. 7 shows the calculated tracer flux per unit cross-section considering or not the electrical double layer (EDL) effect in porous microstructure of clay as the simulation reaches steady state. The temperature difference ΔT equals to $T_{\text{outlet}} - T_{\text{inlet}}$ but the average temperature keeps at the same value $\bar{T} = 0.5(T_{\text{outlet}} + T_{\text{inlet}}) = 323.15 \text{ K}$. If no EDL effect considered, the zeta potential for pore wall of clay is zero. We use chloride ion as tracer to study Soret effect, and the flux with considering EDL is smaller than that without EDL effect due to the negative charged surface of clays. It shows that flux is more sensitive to the temperature gradient in the case where the clay surface is charged. At continue scale, ion transport through porous structures such as clays is usually treated using simplified homogeneous models with macroscale diffusivity and macroscale Soret coefficient. These macroscale parameters are different from those in the free water. Then we calculate the macroscale Soret coefficient by the formula given by Rosanne et al. [19] in the absence of applied electric field:

$$\mathbf{J} = -\bar{D}\nabla\bar{C} - \bar{D}\bar{S}_T\bar{C}\nabla\bar{T}, \quad (19)$$

where \bar{D} and \bar{S}_T denote the macroscale diffusivity and Soret coefficient at continue scale. \bar{C} and \bar{T} are the average concentration and temperature in clays at macroscale. Since we use the constant concentration gradient, the all change of flux is caused by the adjustment of temperature gradient. When temperature difference ΔT is zero, it means $\nabla\bar{T} = 0$ and therefore the macroscale diffusivity can be determined: $\bar{D} = -\mathbf{J}/\nabla\bar{C}$. Then we can use this \bar{D} and the flux changes to calculate \bar{S}_T .

Through simulation, Table 2 gives the values of macroscale Soret coefficients and diffusivities calculated by Eq. (19). If the electrical double layer in clays is considered, the value of the macroscale Soret coefficient for clays is 3.7–11.1 times larger than in the free water, but the macroscale Soret coefficient in porous media without EDL approximately equal to it in free water. These

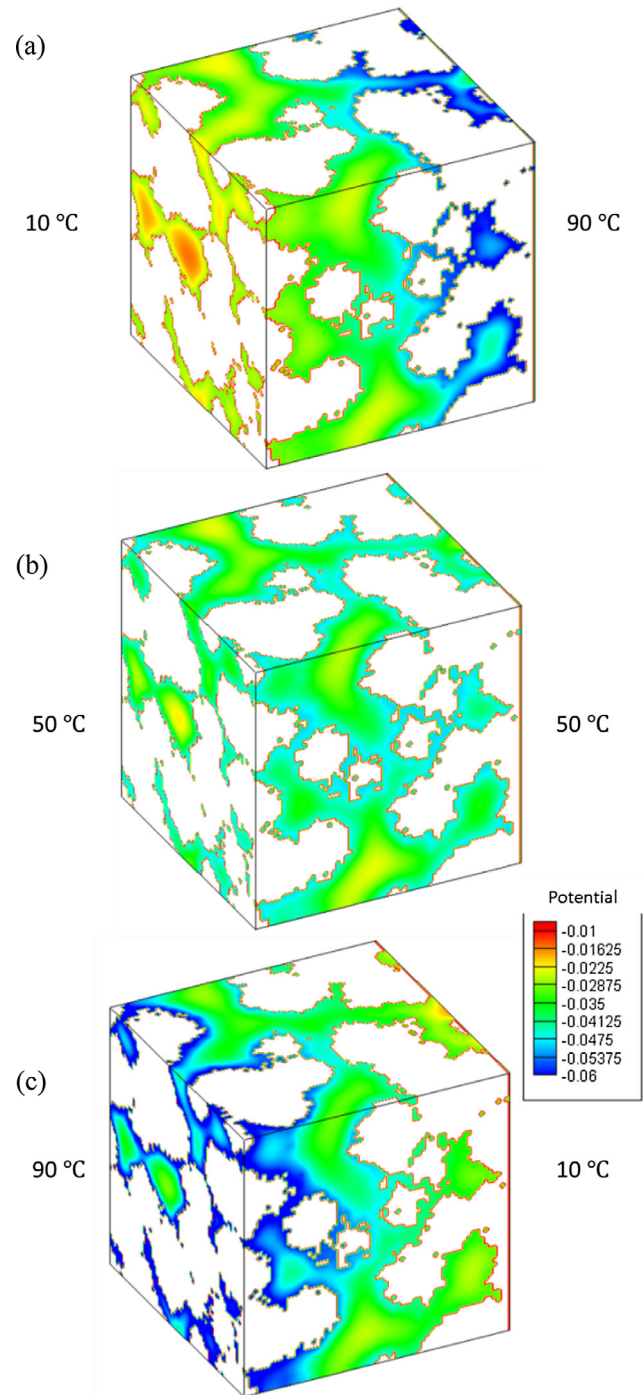


Fig. 6. The electrical potential distribution in porous media for different temperature gradients: (a) $T_{\text{inlet}} = 90^\circ\text{C}$ and $T_{\text{outlet}} = 10^\circ\text{C}$, (b) $T_{\text{inlet}} = 50^\circ\text{C}$ and $T_{\text{outlet}} = 50^\circ\text{C}$, (c) $T_{\text{inlet}} = 10^\circ\text{C}$ and $T_{\text{outlet}} = 90^\circ\text{C}$. The white denotes the solid phase and inhomogeneous potential distributions at pore scale are calculated by our LBM schemes.

results are consistent with the previous research [19]. It seems that the electrokinetic effect could enhance the Soret effect and induce a large value of the Soret coefficient.

Benefiting from the pore-scale simulation, the detail at pore scale can be obtained and therefore we can clarify the flux change from different factors. Considering Eq. (1), the flux comes from three terms: concentration diffusion $-D_i\nabla C_i$, electromigration $-D_i z_i e C_i \nabla \psi / kT$ and thermodiffusion $-D_i S_T C_i \nabla T$. We calculate the mean flux proportions in clays at pore scale shown in Fig. 8. In

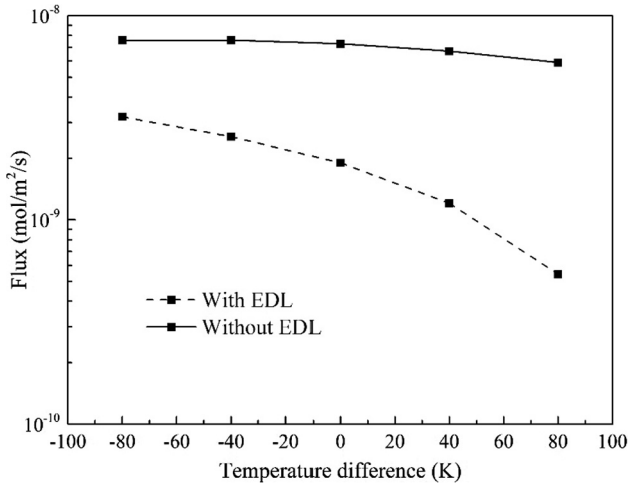


Fig. 7. The tracer flux for different temperature gradient. The temperature difference $\Delta T = T_{\text{outlet}} - T_{\text{inlet}}$. The dash line considers the electrical double layer effect but solid line ignores.

Fig. 8(a), the diffusion and electromigration terms are more sensitive to temperature gradient than thermodiffusion term, but tendencies of diffusion and electromigration with respect to temperature gradient are quite different. The flux from diffusion becomes larger as temperature difference increases, however the opposite trend emerges for electromigration. Hence **Fig. 8(b)** gives the sum of the flux from both diffusion and electromigration over temperature differences. This figure shows direct evidence that the changes of flux by applying different external temperature gradients mainly come from the diffusion and electromigration terms, and the thermodiffusion term has little effect on this change. It means the electrical double layer effect cannot enhance the Soret effect and macroscale Soret coefficient calculated by pore-scale simulation is still around the value for the free water.

The remaining question is why the flux from diffusion and electromigration terms changes so much with the various temperature gradients. The reason lies in the inhomogeneous charged surface induced by applied external temperature gradient. **Fig. 9** shows the mean concentration and potential distributions of each cross section along x direction in clays. The fluctuations of electrical potential and concentration in **Fig. 9** come from the random factors in irregular microstructures of clay. Since the property of surface

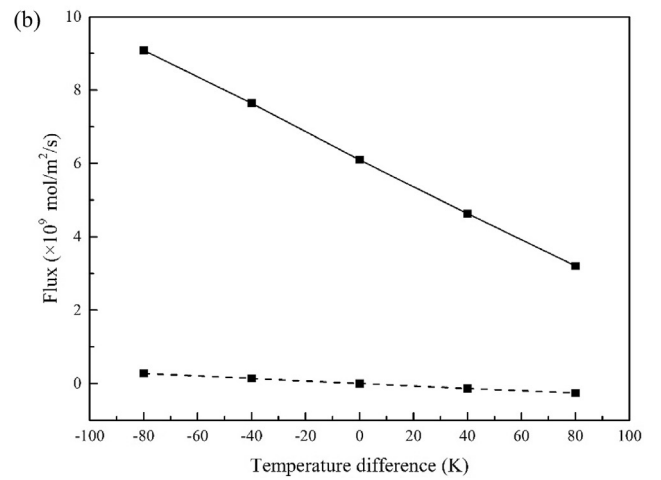
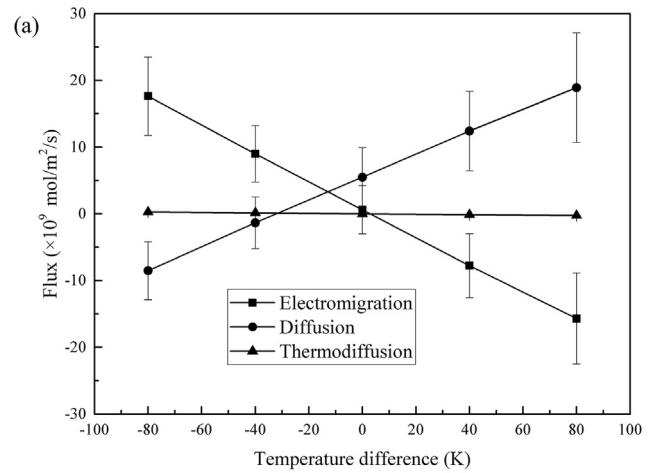


Fig. 8. Flux proportions in clay at pore scale with respect to various temperature differences ΔT are shown in (a); the solid line in (b) is the sum of flux from both diffusion and electromigration, and dash line is the flux from the thermodiffusion. The Soret coefficient is 0.001 K^{-1} .

charge is dependent on the temperature shown in **Fig. 4(a)**, the surface zeta potential is inhomogeneous as the external temperature gradient applied, which induces an inhomogeneous mean electrical potential distribution in clays in **Fig. 9(a)**. Therefore based on

Table 2
The macroscale Soret coefficient and other parameters at different temperature gradients.

	ΔT (K)	S_T (K^{-1})	$-\bar{D}S_T\bar{C}\nabla T^a$ ($\times 10^9 \text{ mol/m}^2/\text{s}$)	\bar{D}^b (m^2/s)	\bar{C}^c ($\times 10^9 \text{ mol/L}$)	\bar{S}_T (K^{-1})	Average \bar{S}_T/S_T	
With EDL	-80	0.001	1.29	1.46×10^{-11}	7.91	0.011	11.1	
	-40		0.66		7.94	0.011		
	0		0.00		7.98	/		
	40		-0.69		7.95	0.011		
	80		-1.36		7.92	0.011		
	-80	0.005	2.34		1.45×10^{-11}	8.14		0.019
	-40		1.15			7.98		0.019
	0		0.00			7.92		/
	40		-1.11			7.91		0.019
	80		-2.18			7.97		0.018
Without EDL	-80	0.001	0.29	5.59×10^{-11}	15.0	0.0003	0.97	
	-40		0.31		15.0	0.0007		
	0		0.00		15.0	/		
	40		-0.58		15.0	0.0013		
	80		-1.38		15.0	0.0015		

^a The total flux J is from our pore-scale simulations and the flux $-\bar{D}S_T\bar{C}\nabla T$ is obtained from Eq. (19).

^b The macroscale diffusivity \bar{D} is calculated as $\Delta T = 0$ by using Eq. (19).

^c The average concentration \bar{C} is from our pore-scale simulations.

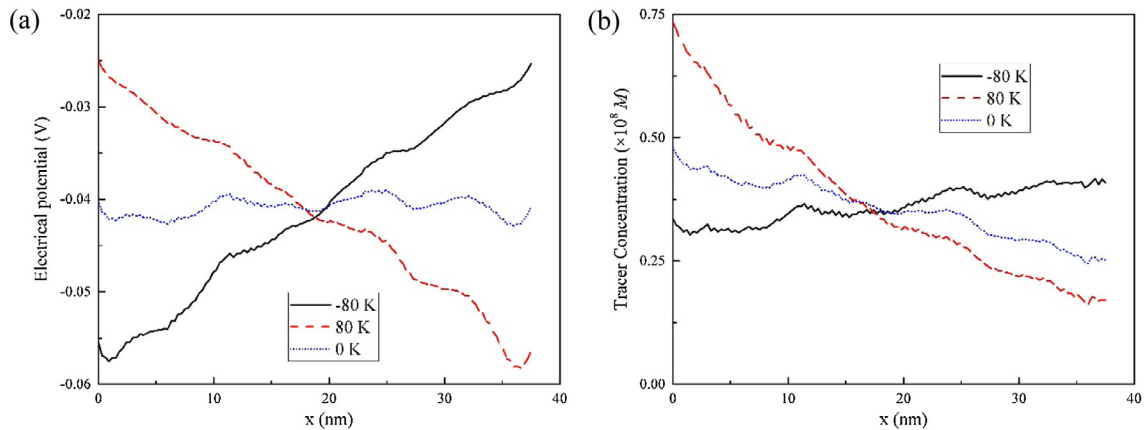


Fig. 9. The mean concentration distribution (a) and potential distribution (b) of cross section along x direction in our simulated domain of clays for various temperature differences. The legends in figures (a) and (b) denote the temperature differences ΔT .

the Donnan equilibrium [41], the inhomogeneous electrical potential in clays would cause the corresponding concentration distribution in Fig. 9(b). When the temperature difference varies from 0 K to 80 K, the mean potential gradient $\nabla\bar{\psi}$ decreases, thus the anionic tracer flux from electromigration term $-D_i z_i e C_i \nabla\bar{\psi} / kT$ also decreases. However the negative charged surface would lower the concentration of anion, hence the tracer's concentration gradient $\nabla\bar{C}$ also decreases but the flux from diffusion term $-D_i \nabla C_i$ will increase. These relations can be easily obtained from the detail information provided by our pore-scale simulation.

As well known, the charged surface of clay would influence the ion distribution in pores by long-rang Coulomb force. Because the pore size of compacted clays is usually comparable with the EDL thickness, the electrical double layer effects, including ion-ion and ion-surface interactions, are very strong and significantly affect ion transport. Therefore, the inhomogeneous charged surface of clay induced by external temperature gradient can also affect flux of ion transport. For instance, the inhomogeneous charged surface generates an inner electrical field in clays, which promotes the ionic electromigration process, but the previous study [19] considers that the electromigration has negligible effect on ion transport because of the absence of external electrical field. Our pore-scale simulation gives the direct evidence that in the thermal chemical coupled transport process the inhomogeneous charge effect in clays has to be regarded as an important role. Despising inhomogeneous charge surface effect will bring the improper conclusions.

5. Conclusions

In this paper, we establish a pore-scale numerical framework to study the ion transport process with electrokinetic effects in porous microstructures of clays. The coupled transport governing equations were solved by a high-efficiency LBM codes on GPU, which has been validated by comparisons with analytic solutions. The present modeling results give a direct evidence to explain why the flux changes so much with an external temperature gradient on saturated clay. In fact, the thermodiffusion has a limited effect on the change of flux in this situation, and the macroscale Soret coefficient of clay is still around the value in free water. The essential cause of the large change of ion flux is the inhomogeneous charged surface induced by the temperature gradient. Although the inhomogeneously charged surface is a solid-liquid interface effect, this effect plays an important role on electrical potential distribution in the pore solution of clay, and then causes the changes of electrical field and concentration field in clay. Therefore the con-

centration diffusion and electromigration should be responsible for this phenomenon instead of the thermodiffusion. The present study could help improve the understanding of thermal-chemical coupled ion transport in clays.

Acknowledgements

This work is financially supported by the NSF grant of China (No. 51676107).

References

- [1] D. Jougnot, A. Revil, P. Leroy, Diffusion of ionic tracers in the Callovo-Oxfordian clay-rock using the Donnan equilibrium model and the formation factor, *Geochim. Cosmochim. Acta* 73 (2009) 2712–2726.
- [2] C. Tournassat, C.A.J. Appelo, Modelling approaches for anion-exclusion in compacted Na-bentonite, *Geochim. Cosmochim. Acta* 75 (2011) 3698–3710.
- [3] I.C. Bourg, G. Sposito, A.C.M. Bourg, Modeling the diffusion of Na⁺ in compacted water-saturated Na-bentonite as a function of pore water ionic strength, *Appl. Geochem.* 23 (2008) 3635–3641.
- [4] T. Gimmi, G. Kosakowski, How mobile are sorbed cations in clays and clay rocks?, *Environ. Sci. Technol.* 45 (2011) 1443–1449.
- [5] C.A.J. Appelo, L.R. Van Loon, P. Wersin, Multicomponent diffusion of a suite of tracers (HTO, Cl, Br, I, Na, Sr, Cs) in a single sample of Opalinus Clay, *Geochim. Cosmochim. Acta* 74 (2010) 1201–1219.
- [6] M. Birgersson, A general framework for ion equilibrium calculations in compacted bentonite, *Geochim. Cosmochim. Acta* 200 (2017) 186–200.
- [7] R.T. Green, S. Painter, Numerical simulation of thermal-hydrological processes observed at the drift-scale heater test at Yucca Mountain, Nevada, in: S. Ove (Ed.), Elsevier Geo-Engineering Book Series, Elsevier, 2004, pp. 175–180.
- [8] S.M. Hsiung, A.H. Chowdhury, M.S. Nataraja, Thermal-mechanical modeling of a large-scale heater test, in: S. Ove (Ed.), Elsevier Geo-Engineering Book Series, Elsevier, 2004, pp. 167–173.
- [9] E.C. Thornton, W.E. Seyfried, Thermodiffusional transport in pelagic clay: implications for nuclear waste disposal in geological media, *Science* 220 (1983) 1156.
- [10] K. Rodríguez, M. Araujo, Temperature and pressure effects on zeta potential values of reservoir minerals, *J. Colloid Interface Sci.* 300 (2006) 788–794.
- [11] M. Martín, J. Cuevas, S. Leguey, Diffusion of soluble salts under a temperature gradient after the hydration of compacted bentonite, *Appl. Clay Sci.* 17 (2000) 55–70.
- [12] H.R. Thomas, M. Sedighi, P.J. Vardon, Diffusive reactive transport of multicomponent chemicals under coupled thermal, hydraulic, chemical and mechanical conditions, *Geotech. Geol. Eng.* 30 (2012) 841–857.
- [13] H. Xie, C. Zhang, M. Sedighi, H.R. Thomas, Y. Chen, An analytical model for diffusion of chemicals under thermal effects in semi-infinite porous media, *Comput. Geotech.* 69 (2015) 329–337.
- [14] A. Revil, C. Meyer, Q. Niu, A laboratory investigation of the thermoelectric effect, *Geophysics* 81 (2016) E243–E257.
- [15] S. Dühr, D. Braun, Why molecules move along a temperature gradient, *Proc. Natl. Acad. Sci. U.S.A.* 103 (2006) 19678–19682.
- [16] J.K. Platten, The Soret effect: a review of recent experimental results, *J. Appl. Mech.* 73 (2005) 5–15.
- [17] R. Rosanne, M. Paszkuta, E. Tevissen, P.M. Adler, Thermodiffusion in compact clays, *J. Colloid Interface Sci.* 267 (2003) 194–203.
- [18] M. Paszkuta, M. Rosanne, P.M. Adler, Transport coefficients of saturated compact clays, *C.R. Geosci.* 338 (2006) 908–916.

- [19] M. Rosanne, M. Paszkuta, P.M. Adler, Thermodiffusional transport of electrolytes in compact clays, *J. Colloid Interface Sci.* 299 (2006) 797–805.
- [20] M. Wang, Q. Kang, Electrochemomechanical energy conversion efficiency in silica nanochannels, *Microfluid. Nanofluid.* 9 (2010) 181–190.
- [21] A. Revil, P.A. Pezard, P.W.J. Glover, Streaming potential in porous media: 1. Theory of the zeta potential, *J. Geophys. Res.: Solid Earth* 104 (1999) 20021–20031.
- [22] M. Taghipoor, A. Bertsch, P. Renaud, Temperature sensitivity of nanochannel electrical conductance, *ACS Nano* 9 (2015) 4563–4571.
- [23] R. Kubo, The fluctuation-dissipation theorem, *Rep. Prog. Phys.* 29 (1966) 255.
- [24] L. Korson, W. Drost-Hansen, F.J. Millero, Viscosity of water at various temperatures, *J. Phys. Chem.* 73 (1969) 34–39.
- [25] U. Kaatze, The dielectric properties of water in its different states of interaction, *J. Solut. Chem.* 26 (1997) 1049–1112.
- [26] C.G. Malmberg, A.A. Maryott, Dielectric Constant of Water from 0 °C to 100 °C, *J. Res. Nat. Bur. Stand.* 56 (1) (1956) 1–8.
- [27] M. Wang, J. Wang, N. Pan, S. Chen, Mesoscopic predictions of the effective thermal conductivity for microscale random porous media, *Phys. Rev. E* 75 (2007) 036702.
- [28] H. Yoshida, T. Kinjo, H. Washizu, Coupled lattice Boltzmann method for simulating electrokinetic flows: a localized scheme for the Nernst-Planck model, *Commun. Nonlinear Sci. Numer. Simul.* 19 (2014) 3570–3590.
- [29] Q. Kang, L. Chen, A.J. Valocchi, H.S. Viswanathan, Pore-scale study of dissolution-induced changes in permeability and porosity of porous media, *J. Hydrol.* 517 (2014) 1049–1055.
- [30] L. Zhang, M. Wang, Modeling of electrokinetic reactive transport in micropore using a coupled lattice Boltzmann method, *J. Geophys. Res. Solid Earth* 120 (2015) 2877–2890.
- [31] F. Kuznik, C. Obrecht, G. Rusaouen, J.-J. Roux, LBM based flow simulation using GPU computing processor, *Comput. Math. Appl.* 59 (2010) 2380–2392.
- [32] P.R. Rinaldi, E.A. Dari, M.J. Vénere, A. Clausse, A Lattice-Boltzmann solver for 3D fluid simulation on GPU, *Simul. Model. Pract. Theory* 25 (2012) 163–171.
- [33] C. Obrecht, F. Kuznik, B. Tourancheau, J.-J. Roux, Scalable lattice Boltzmann solvers for CUDA GPU clusters, *Parallel Comput.* 39 (2013) 259–270.
- [34] H. Yoshida, M. Nagaoka, Multiple-relaxation-time lattice Boltzmann model for the convection and anisotropic diffusion equation, *J. Comput. Phys.* 229 (2010) 7774–7795.
- [35] L. Holzer, B. Münch, M. Rizzi, R. Wepf, P. Marschall, T. Graule, 3D-microstructure analysis of hydrated bentonite with cryo-stabilized pore water, *Appl. Clay Sci.* 47 (2010) 330–342.
- [36] S.J. Altman, W.J. Peplinski, M.L. Rivers, Evaluation of synchrotron X-ray computerized microtomography for the visualization of transport processes in low-porosity materials, *J. Contam. Hydrol.* 78 (2005) 167–183.
- [37] M. Tyagi, T. Gimmi, S.V. Churakov, Multi-scale micro-structure generation strategy for up-scaling transport in clays, *Adv. Water Resour.* 59 (2013) 181–195.
- [38] M. Wang, S. Chen, Electroosmosis in homogeneously charged micro- and nanoscale random porous media, *J. Colloid Interface Sci.* 314 (2007) 264–273.
- [39] L. Zhang, M. Wang, Electro-osmosis in inhomogeneously charged microporous media by pore-scale modeling, *J. Colloid Interface Sci.* 486 (2017) 219–231.
- [40] K.R. Harris, L.A. Woolf, Pressure and temperature dependence of the self diffusion coefficient of water and oxygen-18 water, *J. Chem. Soc., Faraday Trans. 1: Phys. Chem. Condens. Phases* 76 (1980) 377–385.
- [41] H. Tian, L. Zhang, M. Wang, Applicability of Donnan equilibrium theory at nanochannel-reservoir interfaces, *J. Colloid Interface Sci.* 452 (2015) 78–88.